
Titanium Oxides and Silicates as High- κ Dielectrics: A First-Principles Investigation

G.-M. RIGNANESE,¹ X. ROCQUEFELTE,¹ X. GONZE,¹
ALFREDO PASQUARELLO²

¹Unité de Physico-Chimie et de Physique des Matériaux, Université Catholique de Louvain, 1 Place Croix du Sud, B-1348 Louvain-la-Neuve, Belgium, and Research Center on Microscopic and Nanoscopic Materials and Electronic Devices (CERMIN), Université Catholique de Louvain, B-1348 Louvain-la-Neuve, Belgium

²Institut de Théorie des Phénomènes Physiques (ITP), Ecole Polytechnique Fédérale de Lausanne (EPFL), CH-1015 Lausanne, Switzerland, and Institut Romand de Recherche Numérique en Physique des Matériaux (IRRMA), CH-1015 Lausanne, Switzerland

Received 6 October 2003; accepted 27 February 2004

Published online 3 November 2004 in Wiley InterScience (www.interscience.wiley.com).

DOI 10.1002/qua.20339

ABSTRACT: Using density functional theory, we investigate the structural, vibrational, and dielectric properties of titanium oxides and silicates, which have attracted considerable attention in the framework of the quest for alternative high- κ materials. For the oxides, three crystalline phases of titanium dioxide are considered. The first two are hypothetical; they are obtained by similarity with the cubic and tetragonal structure of zirconia ZrO_2 or hafnia HfO_2 . The third is the rutile, a crystal that occurs naturally. For the silicates, we analyze a hypothetical $TiSiO_4$ structure constructed by analogy with crystalline $ZrSiO_4$ and $HfSiO_4$ (zircon and hafnon).

© 2004 Wiley Periodicals, Inc. Int J Quantum Chem 101: 793–801, 2005

Key words: high- κ dielectrics; transition metal oxides; silicates; vibrational properties; dielectric properties

For the last 10 years, the Semiconductor Industry Association (SIA) has been publishing road maps for semiconductor technology [1]. These basically affirm the desire of the industry to continue with Moore's law [2], which is often stated as

Correspondence to: G.-M. Rignanese; e-mail: rignanese@pcpm.ucl.ac.be

the doubling of transistor performance and quadrupling of the number of devices on a chip every three years. This phenomenal progress has been achieved through the scaling of the metal-oxide-semiconductor field-effect transistor (MOSFET) to smaller and smaller physical dimensions [3].

The narrowest feature on present-day integrated circuits is the gate oxide, the thin dielectric layer

that forms the basis of field-effect device structures. So far, silicon dioxide has been the dielectric of choice. The SIA's road map indicates that the equivalent thickness¹ of the gate dielectric will need to be 10 to 15 Å by 2004. As a result of increased power consumption, intrinsic device reliability, and circuit instabilities associated with silicon dioxide of such a small thickness (about 5 silicon atoms across), an alternative high-permittivity (high- κ) gate dielectric with low leakage current and at least equivalent capacitance, performance, and reliability is required. Considerable research has been dedicated to the study of potential dielectric-gate material candidates.

Replacing the SiO₂ with a material having a different dielectric constant is not as simple as it may seem. The material bulk and interface properties must be comparable to those of silicon dioxide, which are remarkably good. For instance, thermodynamic stability with respect to silicon, stability under thermal conditions relevant to microelectronic fabrication, low diffusion coefficients, and thermal expansion match are quite critical.

Recent research on high- κ dielectrics has primarily focused on metal oxides and their silicates [4]. Among these, the group IVb transition metals Ti, Zr, and Hf have generated a substantial amount of investigations [5]. In particular, titanium dioxide, which is known to exhibit dielectric constants of 80–110 depending on the crystal structure, is a prime candidate for gate dielectrics [5–8]. Recently, titanium silicates have also been considered as a potential alternative for SiO₂ [9–11].

The dielectric properties of these materials constitute an issue of great practical relevance. In particular, it would be helpful to understand the relation between the permittivity and the underlying microstructure. In this framework, first-principles calculations can provide useful indications, given that relatively little experimental data are available. So far, first-principles studies of the dielectric properties of high- κ materials [12–18] have focused on Zr and Hf oxides and silicates. In particular, it was shown that the chemical homology of zirconium and hafnium leads to similar properties for their oxides and silicates. The aim of the present study is

¹ For a given gate oxide with a dielectric constant (κ), the term equivalent thickness (t_{eq}) represents the theoretical thickness of SiO₂ that would be required to achieve the same capacitance density as the dielectric. If κ is substantially higher than that of SiO₂ (κ_{ox}) a much smaller equivalent thickness will be achieved even with a larger physical thickness (t_{phys}): $t_{\text{eq}} = \kappa_{\text{ox}}/\kappa t_{\text{phys}}$.

to extend these calculations to titanium-based materials. Although the chemistry of the 4d and 5d elements (such as Zr and Hf) is very similar, it should be considerably different for the 3d metals (such as Ti).

Using density functional theory (DFT), we investigate various model crystalline structures of Ti oxides and silicates. We compute the phonon frequencies at the Γ point of the Brillouin zone, the Born effective charge tensors,² and the dielectric permittivity tensors. As a side question, we also discuss the similarities and the differences related to the three group IVb metals: Ti, Zr, and Hf.

The article is organized as follows. After a brief account of the technical details in Section I, we describe our four crystalline model structures (three oxides and one silicate) and study their structural properties in Section II. The Born effective charge tensors are analyzed in detail in Section III. The phonon frequencies at the Γ point of the Brillouin zone are presented in Section IV, and the dielectric permittivity tensors are discussed in Section V. Finally, in Section VI, we summarize our results and conclude.

I. Technical Details

All our calculations are performed using the ABINIT package, developed by the authors and collaborators [20]. The exchange-correlation energy is evaluated within the local density approximation (LDA) to DFT, using Perdew and Wang's parameterization [21] of Ceperley–Alder electron-gas data [22].

Only valence electrons are explicitly considered using pseudopotentials to account for core-valence interactions. We use norm-conserving pseudopotentials [23, 24] with Ti (3s, 3p, 3d, 4s), Si (3s, 3p), and O (2s, 2p) levels treated as valence states.

The wave functions are expanded in plane waves up to a kinetic energy cutoff of 45 Ha. For each phase, the Brillouin zone is sampled by a Monkhorst–Pack [25] mesh of k -points.³ The chosen kinetic energy cutoff and k -point sampling of the

² In quantum chemistry, the Born effective charge tensors are usually known as “atomic polar tensors” (see, e.g., Ref. [19]).

³ For c-TiO₂, t-TiO₂, and TiSiO₄, our mesh corresponds to a 4 × 4 × 4 grid in the conventional unit cell, leading to 10, 12, and 15 special k -points in the irreducible Brillouin zone, respectively. For r-TiO₂, we use a 4 × 4 × 6 grid that results in 9 special k -points in the irreducible Brillouin zone.

Brillouin zone ensure convergence of all the calculated properties.

II. Structural Properties

To investigate the dielectric properties of the titanium oxides and silicates, we examine a set of crystalline structures, which are reproduced in Figure 1. To model the oxides, we first consider the hypothetical cubic and tetragonal phases, *c*-TiO₂ and *t*-TiO₂ respectively, obtained by analogy with the corresponding phases of HfO₂ and ZrO₂.

In the cubic phase, represented in Figure 1(a), TiO₂ takes the fluorite structure (space group *Fm* $\bar{3}$ *m*), which is fully characterized by a single lattice constant *a*. The Ti atoms are in a face-centered-cubic (fcc) structure and the O atoms occupy the tetrahedral interstitial sites associated with this fcc lattice. The primitive unit cell contains one formula unit of TiO₂, whereas the conventional unit cell has four of them.

The tetragonal phase (space group *P4*₂/*nmc*) can be viewed as a distortion of the cubic structure obtained by displacing alternating pairs of O atoms up and down by an amount Δz along the *z* direction, as marked by the arrows in Figure 1(b), and by applying a tetragonal strain. The resulting primitive cell is doubled compared to the cubic phase,

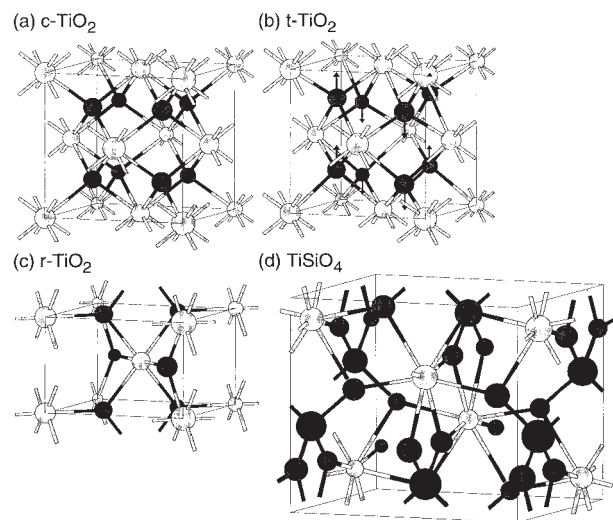


FIGURE 1. Ball and stick representation of our four model structures of titanium oxides and silicates: (a) cubic TiO₂, (b) tetragonal TiO₂, (c) rutile TiO₂, and (d) TiSiO₄. The Ti, O, and Si atoms are colored in light, medium, and dark grey, respectively.

including two formula units of TiO₂. The conventional unit cell, reproduced in Figure 1(b), has four formula units of TiO₂. The tetragonal structure is completely specified by two lattice constants (*a* and *c*) and the dimensionless ratio $d_z = \Delta z/c$ describing the displacement of the O atoms. The cubic phase can be considered as a special case of the tetragonal structure with $d_z = 0$ and $c/a = 1$ (if the primitive cell is used for the tetragonal phase, $c/a = \sqrt{2}$).

We also investigate the rutile phase, *r*-TiO₂, which occurs naturally. The rutile structure (space group *P4*₂/*mmm*) has a tetragonal unit cell with two formula units of TiO₂. The Ti atoms occupy the body-centered-cubic positions and the O atoms are at (*u*, *u*, 0), (1 - *u*, 1 - *u*, 0), (1/2 - *u*, 1/2 + *u*, 1/2), and (1/2 + *u*, 1/2 - *u*, 1/2), as reported in Figure 1(c). The rutile structure is completely specified by two lattice constants (*a* and *c*) and the internal parameter *u* related to the positions of O atoms.

The *r*-TiO₂ is found to be the most stable of these three models. At variance, for Zr- and Hf-based oxides, the tetragonal structure is the most stable. It is interesting to note that in the rutile phase the M = (Ti, Zr, Hf) atoms are sixfold coordinated, but in the cubic and tetragonal phases they are eightfold coordinated. This is a first clear difference between Ti atoms, on the one hand, and Zr and Hf atoms, on the other. It can be related to the smaller ionic radius of Ti⁴⁺ (0.61 [26]) compared to Zr⁴⁺ and Hf⁴⁺ (0.72 and 0.71 Å, respectively [26]).

To simulate the silicates, we consider the TiSiO₄ crystal defined by similarity with hafnon and zircon. It has a conventional unit cell which is body-centered tetragonal (space group *I4*₁/*amd*) and contains four formula units of TiSiO₄, as illustrated in Figure 1(d). A primitive cell containing only two formula units of TiSiO₄ can also be defined. The positions of the Ti and Si atoms are imposed by symmetry: they are located at (0, 3/4, 1/8) and (0, 1/4, 3/8) on the 4a and 4b Wyckoff sites, respectively. The O atoms occupy the 16th Wyckoff sites (0, *u*, *v*), where *u* and *v* are internal parameters.

In terms of the bonding environment of the various atomic species, the four models are very different. In *r*-TiO₂, the Ti atoms are sixfold coordinated to O atoms that are threefold coordinated. In TiSiO₄, the Ti atoms are eightfold coordinated to O atoms that are threefold coordinated. In *c*-TiO₂ and *t*-TiO₂, the Ti atoms are also eightfold coordinated but the O atoms are fourfold coordinated.

The calculated structural parameters of *c*-TiO₂, *t*-TiO₂, *r*-TiO₂, and TiSiO₄ are reported in Table I.

TABLE I
Calculated structural parameters of c-TiO₂, t-TiO₂, r-TiO₂, and TiSiO₄.

	c-TiO ₂	t-TiO ₂	r-TiO ₂	TiSiO ₄
Lattice constants				
<i>a</i>	4.72	4.71	4.53	6.21
<i>c</i>		4.93	2.92	5.81
Volume				
<i>V</i>	26.29	27.34	60.12	112.03
Internal parameters				
<i>u</i>			0.3033	0.0591
<i>v</i>				0.1892
<i>d_z</i>		0.0701		
Interatomic distances				
Ti—O	2.04	1.89 2.29	1.93 1.94	1.95 2.19

Length in Å.

Our results for r-TiO₂ agree well with experiment [27] and a previous DFT calculation [28].

Although it was found that the structural parameters for Zr- and Hf-based oxides and silicates are very similar [18], the values for Ti-based materials can differ by about 5–10% from the former two. The largest difference is found in the tetragonal phase the Ti—O distance is found to be 10 and 13% smaller than the Zr—O and Hf—O distances, respectively. This is another evidence of the different

chemistry of 3d metals with respect to 4d and 5d metals.

III. Born Effective Charge Tensors

For insulators, the Born effective charge tensor [19] $Z_{\kappa,\beta\alpha}^*$ is defined as the proportionality coefficient relating, at linear order, the polarization per unit cell, created along the direction β , and the displacement along the direction α of the atoms belonging to the sublattice κ , under the condition of zero electric field. The same coefficient also describes the linear relation between the force on an atom and the macroscopic electric field. The Born effective charge tensors are connected to the mixed second-order derivative of the energy with respect to atomic displacements and macroscopic electric field [29]. The Born effective charge tensors of Ti, Si, and O atoms for the four crystalline structures are reported in Table II.

Because of the symmetry of the cubic phase, the Born effective charge tensors of Ti and O atoms are diagonal and isotropic. The value of Z^* is anomalously large for Ti atoms compared to the nominal ionic charge $Z = 4$. This behavior has also been observed in the case of c-ZrO₂ and c-HfO₂ [14, 15, 18]. A detailed analysis of the physics of Born effective charges in the case of perovskite ferroelectrics (like PbZrO₃) ascribed this effect to a mixed covalent-ionic bonding [30].

In the tetragonal structure, the symmetry imposes that the Born effective charge tensor of Ti

TABLE II
Calculated Born effective charge tensors for Ti, Si, and O atoms in c-TiO₂, t-TiO₂, r-TiO₂, and TiSiO₄.

Atom	c-TiO ₂	t-TiO ₂	r-TiO ₂	TiSiO ₄
Ti	$\begin{pmatrix} +6.40 & 0 & 0 \\ 0 & +6.40 & 0 \\ 0 & 0 & +6.40 \end{pmatrix}$	$\begin{pmatrix} +6.63 & 0 & 0 \\ 0 & +6.63 & 0 \\ 0 & 0 & +4.42 \end{pmatrix}$	$\begin{pmatrix} +6.36 & +1.00 & 0 \\ +1.00 & +6.36 & 0 \\ 0 & 0 & +7.52 \end{pmatrix}$	$\begin{pmatrix} +5.91 & 0 & 0 \\ 0 & +5.91 & 0 \\ 0 & 0 & +4.01 \end{pmatrix}$
Si				$\begin{pmatrix} +3.56 & 0 & 0 \\ 0 & +3.56 & 0 \\ 0 & 0 & +4.83 \end{pmatrix}$
O	$\begin{pmatrix} -3.20 & 0 & 0 \\ 0 & -3.20 & 0 \\ 0 & 0 & -3.20 \end{pmatrix}$	$\begin{pmatrix} -4.76 & 0 & 0 \\ 0 & -1.94 & 0 \\ 0 & 0 & -2.21 \end{pmatrix}$	$\begin{pmatrix} -3.18 & -1.81 & 0 \\ -1.81 & -3.18 & 0 \\ 0 & 0 & -3.76 \end{pmatrix}$	$\begin{pmatrix} -1.20 & 0 & 0 \\ 0 & -3.54 & -0.11 \\ 0 & -0.45 & -2.22 \end{pmatrix}$

For c-TiO₂ and t-TiO₂, the Born effective charge tensors for oxygen atoms are the same, whatever their location, whereas for r-TiO₂ and TiSiO₄, they depend on the positions of the O atoms. The tensors presented for r-TiO₂ and TiSiO₄ refer to O atoms located at (*u*, *u*, 0) and (0, *u*, *v*), respectively. The Born effective charge tensors for the other oxygen atoms can be obtained using the symmetry operations.

atoms is diagonal and only has two independent components: parallel (Z_{\parallel}^*) and perpendicular (Z_{\perp}^*) to the c axis. The tensor is very anisotropic: the value of Z_{\perp}^* is 3% larger than the one calculated for the cubic phase, whereas Z_{\parallel}^* is more than 30% smaller. This is another manifestation of the different behavior of Ti atoms compared to Zr and Hf atoms. Indeed, in their tetragonal oxides, the Born effective charge tensors of Zr and Hf atoms were found to be quite isotropic [14, 15, 18]. The Born effective charge tensor of the O atoms is also diagonal, but with three independent components. It is even more anisotropic than the tensor of Ti atoms: the ratio between the largest and the smallest components is about 2.5. This ratio is only 1.6 for t-ZrO₂ and 1.4 for t-HfO₂. Such a strong anisotropy of the Born effective charge tensor of O atoms has already been observed in SiO₂-stichovite [31] and TiO₂-rutile [28].

In the rutile structure, the Born effective charge tensors of Ti or O atoms have only three independent components: Z_{xx}^* , Z_{xy}^* , and Z_{zz}^* . Indeed, Z_{yy}^* and Z_{yx}^* are equal to Z_{xx}^* and Z_{xy}^* , respectively, and the other components are zero. Our calculated Born effective charge tensors agree well with those of a previous DFT calculation [28]. When we take a coordinate system whose axes are along the [110], $\bar{1}\bar{1}0$, and [001] directions, the tensors are diagonalized. In this coordinate system, the principal values are (+7.35, +5.36, +7.52) for Ti atoms and (-4.99, -1.37, -3.76) for O atoms. In this latter case, the ratio between the largest and the smallest components is about 3.6. The anisotropy is even larger than in the tetragonal phase.

In the TiSiO₄ structure, the local site symmetry of Ti and Si atoms is rather high ($\bar{4}m2$). The born effective charge tensors of Ti and Si atoms are diagonal and have only two independent components: parallel and perpendicular to the tetragonal axis, Z_{\parallel}^* and Z_{\perp}^* , respectively. The local site symmetry of the O atoms has only a mirror plane. As a consequence, the Born effective charge tensors of O atoms are not diagonal and depend on five independent quantities. We examine the tensor for the O atom located at (0, u , v), which is reported in Table II. The Born effective charge tensors of the other oxygen atoms can be obtained using the symmetry operations. For this particular atom, the mirror plane is perpendicular to x . Note that Z_{yz}^* and Z_{zy}^* are different, but rather small, making the Born effective charge tensor almost diagonal. To characterize the anisotropy of this tensor, we select its symmetric part and diagonalize it. The principal

values are (-1.20, -3.60, -2.16) and the principal direction associated to the largest principal value forms an angle of about 18° to the y axis.

On the one hand, the largest component of the Born effective charge tensors and the strongest anisotropy are found in the rutile phase. On the other hand, the TiSiO₄ phase is the one for which the components of the Born effective charge tensors are the closest to their nominal values. These differences can be related to the different bonding environment in the various systems (see Section II).

IV. Phonon Frequencies at the Γ Point

The theoretical group analysis [32] predicts the following irreducible representations of optical and acoustical zone-center modes:

$$\Gamma_{c\text{-TiO}_2} = \underbrace{F_{2g}}_{\text{Raman}} \oplus \underbrace{F_{1u}}_{\text{IR}} \oplus \underbrace{F_{1u}}_{\text{Acoustic}}$$

$$\Gamma_{t\text{-TiO}_2} = \underbrace{A_{1g} \oplus 2B_{1g} \oplus 3E_g}_{\text{Raman}} \oplus \underbrace{A_{2u} \oplus 2E_u}_{\text{IR}} \\ \oplus \underbrace{A_{2u} \oplus E_u}_{\text{Acoustic}} \oplus \underbrace{B_{2u}}_{\text{Silent}}$$

$$\Gamma_{r\text{-TiO}_2} = \underbrace{A_{1g} \oplus B_{1g} \oplus B_{2g} \oplus E_g}_{\text{Raman}} \oplus \underbrace{A_{2u} \oplus 3E_u}_{\text{IR}} \\ \oplus \underbrace{A_{2u} \oplus E_u}_{\text{Acoustic}} \oplus \underbrace{A_{2g} \oplus 2B_{1u}}_{\text{Silent}}$$

$$\Gamma_{\text{TiSiO}_4} = \underbrace{2A_{1g} \oplus 4B_{1g} \oplus B_{2g} \oplus 5E_g}_{\text{Raman}} \oplus \underbrace{3A_{2u} \oplus 4E_u}_{\text{IR}} \\ \oplus \underbrace{A_{2u} \oplus E_u}_{\text{Acoustic}} \oplus \underbrace{B_{1u} \oplus A_{2g} \oplus A_{1u} \oplus 2B_{2u}}_{\text{Silent}}$$

Although the space group differ for t-TiO₂, r-TiO₂, and TiSiO₄, their point group ($4/mmm$) is the same. Hence the same notations appear in the irreducible representations of the zone-center modes.

Because of the nonvanishing components of the Born effective charge tensors, the dipole-dipole interaction must be properly included in the calculation of the interatomic force constants [29, 33, 34]. In particular, the dipole-dipole contribution is found to be responsible for the splitting at the Γ point between the longitudinal and transverse optic (LO

TABLE III
Fundamental frequencies of c-TiO₂, t-TiO₂, r-TiO₂, and TiSiO₄ (in cm⁻¹) with their symmetry assignments. In t-TiO₂, the E_u mode with an imaginary frequency tends to break the symmetry imposed in the calculation and implies an instability of the structure.

Mode	c-TiO ₂	t-TiO ₂	r-TiO ₂	TiSiO ₄
Raman				
A _{1g} (1)		381.6	636.2	383.2
A _{1g} (2)				1011.4
B _{1g} (1)		351.2	115.7	258.9
B _{1g} (2)		668.6		417.6
B _{1g} (3)				627.2
B _{1g} (4)				1047.2
B _{2g}			844.1	262.9
E _g (1)		130.4	481.1	194.3
E _g (2)		435.2		242.4
E _g (3)		730.6		430.1
E _g (4)				544.3
E _g (5)				945.4
F _{2g}	618.6			
Infrared				
A _{2u} (TO1)		429.0	204.3	318.7
A _{2u} (LO1)		678.0	779.1	482.4
A _{2u} (TO2)				606.4
A _{2u} (LO2)				630.5
A _{2u} (TO3)				1000.3
A _{2u} (LO3)				1106.1
E _u (TO1)		116.0i	179.9	303.4
E _u (LO1)		165.8	354.1	374.0
E _u (TO2)		496.3	404.1	374.1
E _u (LO2)		850.1	448.2	414.1
E _u (TO3)			502.2	433.1
E _u (LO3)			824.7	496.8
E _u (TO4)				876.7
E _u (LO4)				1047.6
F _{1u} (TO)	176.5			
F _{1u} (LO)	685.5			
Silent				
B _{1u} (1)			125.7	124.7
A _{2g}			419.3	250.1
A _{1u}				418.3
B _{1u} (2)			423.0	
B _{2u} (1)		660.1		547.3
B _{2u} (2)				969.2

and TO, respectively) modes F_{1u} in c-TiO₂, E_u (perpendicular to c) and A_{2u} (parallel to c) in t-TiO₂, r-TiO₂, TiSiO₄.

The calculated phonon frequencies are reported in Table III. Our results for r-TiO₂ differ by less than 2–3% from those of another first-principles calcula-

tion [28]. In t-TiO₂, one E_u mode has an imaginary frequency. This corresponds to a negative curvature of the total energy dependence on the atomic positions, hence to a saddle point. This vibration mode tends to break the symmetry imposed in the calculation. Hence, the tetragonal structure is found to be unstable.

The lowest infrared active modes are found for the cubic and the rutile phases at about 180 cm⁻¹ (F_{1u} mode in c-TiO₂, and the first E_u mode in r-TiO₂). Comparatively, the lowest infrared mode in TiSiO₄ presents a much higher frequency (about 300 cm⁻¹). This will have a direct effect on the contributions to static permittivity tensors, as we will discuss hereafter.

The atomic motions associated to the various vibrational modes have been described in detail in the literature. The interested reader will refer to Refs. [35–37] for c-TiO₂ and t-TiO₂, Ref. [30] for r-TiO₂, and Refs. [12, 38] for TiSiO₄.

V. Dielectric Permittivity Tensors

The calculated values of ϵ_∞ and ϵ_0 are reported in Table IV. In the tetragonal phase, the instability found for the E_u mode precludes the calculation of ϵ_0 . In the cubic phase, the electronic (ϵ_∞) and static (ϵ_0) permittivity tensors are diagonal and isotropic. In the other three crystals, the tensors are still diagonal by symmetry, but have two independent components $\epsilon_{||}$ and ϵ_{\perp} , parallel and perpendicular to the c axis, respectively.

For a deeper analysis of the static dielectric tensor, we can rely not only on the frequencies of the IR-active modes, but also on the corresponding eigendisplacements and Born effective charges. Indeed, the static dielectric tensor can be decomposed in the contributions of different modes as follows (see Ref. [39]; we follow the notations of Ref. [29]):

$$\epsilon_{\alpha\beta}^0(\omega) = \epsilon_{\alpha\beta}^\infty + \sum_m \Delta\epsilon_{m,\alpha\beta} = \epsilon_{\alpha\beta}^\infty + \frac{4\pi}{\Omega_0} \sum_m \frac{S_{m,\alpha\beta}}{\omega_m^2}, \quad (1)$$

where Ω_0 is the volume of the primitive unit cell. $S_{m,\alpha\beta}$ is the mode-oscillator strength, related to the eigendisplacements $U_m(\kappa\alpha)$ and the Born effective charge tensors by

$$S_{m,\alpha\beta} = \left(\sum_{\kappa\alpha'} Z_{\kappa,\alpha\alpha'}^* U_m^*(\kappa\alpha') \right) \left(\sum_{\kappa'\beta'} Z_{\kappa',\beta\beta'} U_m(\kappa'\beta') \right). \quad (2)$$

TABLE IV
Electronic and static dielectric tensors of c-TiO₂, t-TiO₂, r-TiO₂, and TiSiO₄.*

	c-TiO ₂	t-TiO ₂		r-TiO ₂		TiSiO ₄	
			⊥		⊥		⊥
ε _∞	9.11	6.66	8.81	8.57	7.49	5.52	5.56
Δε ₁	128.36			116.16	81.65	9.90	11.54
Δε ₂					2.90	0.31	0.00
Δε ₃					5.23	1.01	0.46
Δε ₄							1.88
ε ₀	137.47			124.74	96.28	16.73	19.44

* The static dielectric tensor for t-TiO₂ cannot be calculated because of the instability of the phase (see discussion in the text). In all cases, the tensors are diagonal. For the cubic phase, it is also isotropic; for the other three phases, the tensors have different components parallel (||) and perpendicular (⊥) to the *c* axis. The contribution of each of the IR-active modes for c-TiO₂, r-TiO₂, and TiSiO₄ are also indicated. In c-TiO₂, the contribution originates from the *F*_{1*u*} mode. In r-TiO₂ and TiSiO₄, the phonon mode contributions to ε₀^{||} come from the *A*_{2*u*} modes, while the contributions to ε₀[⊥] are related to the *E*_{*u*} modes.

Displacements are normalized according to the condition

$$\sum_{\kappa\beta} M_{\kappa} [U_m(\kappa\beta)]^* U_n(\kappa\beta) = \delta_{mn}, \quad (3)$$

where *M*_κ is the mass of the ion κ.

The contribution of the individual modes Δε_{*m*} to the static dielectric constant are indicated in Table IV (except for the t-TiO₂ phase), while the oscillator strength tensors are reported in Table V. This tensor is isotropic for the *F*_{1*u*} mode in the cubic phase. For the other phases, it is necessary to distinguish the

TABLE V
Components of the oscillator strength tensor *S*_{*m*} for each of the IR-active modes for c-TiO₂, t-TiO₂, r-TiO₂, and TiSiO₄.

	c-TiO ₂ <i>S</i> _{<i>m</i>}	t-TiO ₂ <i>S</i> _{<i>m</i>}	r-TiO ₂ <i>S</i> _{<i>m</i>}	TiSiO ₄ <i>S</i> _{<i>m</i>}
<i>A</i> _{2<i>u</i>} (1)		11.18	32.33	12.53
<i>A</i> _{2<i>u</i>} (2)				1.41
<i>A</i> _{2<i>u</i>} (3)				12.49
<i>E</i> _{<i>u</i>} (1)		6.20	17.62	13.22
<i>E</i> _{<i>u</i>} (2)		20.91	3.17	0.00
<i>E</i> _{<i>u</i>} (3)			7.12	1.08
<i>E</i> _{<i>u</i>} (4)				18.05
<i>F</i> _{1<i>u</i>}	11.69			

The description of the tensor's structures corresponding to the various types of modes is given in the text.

The oscillator strengths are presented in 10⁻⁴ au (1 au = 0.342036 m³/s²).

directions parallel and perpendicular to the tetragonal axis for the *A*_{2*u*} and *E*_{*u*} modes. We indicate the parallel-parallel component for the *A*_{2*u*} mode, and the perpendicular-perpendicular component for the *E*_{*u*} modes.

For each symmetry representation (*A*_{2*u*} and *E*_{*u*}), the lowest and highest frequency modes exhibit the largest oscillator strengths. Despite their similar oscillator strengths, the modes of lowest frequency contribute much more to the static dielectric constant than the modes of highest frequency, the frequency factor in Eq. (1) playing a crucial role. That is particularly true for the c-TiO₂ compared to c-ZrO₂ and c-HfO₂. In this case, the frequency of the *F*_{1*u*} mode in the titanium oxide is more than 35% smaller than in the other two oxides. This reduced frequency as well as the increased Born effective charge (see discussion in Section III) leads to a static dielectric constant more than 4 times larger in c-TiO₂.

In TiSiO₄, this effect is much less pronounced so that ε₀ is considerably smaller than in c-TiO₂ and r-TiO₂. For TiSiO₄, we find theoretical values of 16.73 and 19.44 for ε₀^{||} and ε₀[⊥], respectively. The only available experimental data for Ti silicates have been obtained for deposited amorphous films [10]. Values ranging from 11 to 16 are found. However, these numbers should be taken with great caution given the possible presence of interfacial oxides, which contribute to reducing the dielectric constant of the film. Regarding our theoretical values, it should be noted that the LDA to density functional theory tends to overestimate ε_∞ by about 10%, meaning an overestimation of ε₀ by 2 or 3%. Be-

sides, it has been proposed recently that the anomalous part of the Born effective charges might be exaggerated within LDA if self-interaction corrections are not explicitly taken into account [40]. Hence the resulting contributions $\Delta\epsilon_m$ are also overestimated. Globally, it can be considered that the agreement between our results and experiments is quite reasonable.

It is also interesting to note that the static dielectric constant is found to be larger in *c*-TiO₂ than in *r*-TiO₂, that is when Ti atoms are eightfold coordinated rather than sixfold. On the contrary, for Zr atoms, it has been found in a previous first-principles study [17] that ZrO₆ structural units contribute the most to the static dielectric constant. Here, when Ti atoms are eightfold coordinated, there exist a very soft mode (it can be so soft that the structure becomes unstable in the case of the tetragonal phase) that contributes to increasing ϵ_0 very significantly. This difference can again be related to the smaller ionic radii for Ti⁴⁺ as discussed in Section II.

VI. Conclusion

Using DFT, we have investigated the structural, dynamical, and dielectric properties of Ti oxides and silicates, which are very promising high- κ alternatives to the conventional SiO₂ gate dielectric. We have considered three crystalline oxides (the hypothetical cubic and tetragonal phases built by analogy with hafnia and zirconia phases, and the naturally occurring rutile phase) and one crystalline silicate similar to hafnon and zircon.

The structural properties of these different phases have been calculated and discussed. The rutile phase is found to be the most stable oxide at variance with ZrO₂ and HfO₂ for which the tetragonal phase is more stable. This different behavior can be related to the smaller ionic radius of Ti⁴⁺ compared to Zr⁴⁺ and Hf⁴⁺.

The Born effective charge tensors have been analyzed in detail showing anomalously large values for Ti and O atoms compared to their nominal values. In *t*-TiO₂ and *r*-TiO₂, a strong anisotropy was found in the Born effective charge tensors of O atoms, indicating a mixed covalent-ionic bonding between Ti and O.

The phonon frequencies at the center of the Brillouin zone have been computed. The cubic and the rutile phases show an infrared-active mode with a very low frequency. The *t*-TiO₂ structure was

found to be unstable, with a vibration mode that tends to break the symmetry imposed in the calculation.

The electronic and static dielectric permittivity tensors have also been determined within perturbation DFT. A detailed analysis of the contributions of the different vibrational modes has been performed (except for *t*-TiO₂), including computation of the oscillator strength tensors. Our analysis reveals that when Ti atoms are eightfold coordinated to O atoms (like in *c*-TiO₂) rather than sixfold (like in *r*-TiO₂), a very soft mode significantly contributes to increasing the static dielectric constant. Trying to stabilize this type of bonding environment might be an interesting way to improve the dielectric properties of high- κ dielectrics.

ACKNOWLEDGMENTS

"G. M. R. and X. G. are grateful to the National Fund for Scientific Research (FNRS) of Belgium for financial support. Parts of this work are also directly connected to the Belgian Program on Interuniversity Attraction Poles (PAI5/1/1) on Quantum Size Effects in Nanostructured Materials, to the Action de Recherche Concertée entitled "Interaction électron-phonon dans les nanostructures" sponsored by the Communauté Française de Belgique. A. P. acknowledges support from the Swiss National Science Foundation (Grant No. 620-57850.99).

References

1. <http://public.itrs.net>
2. Moore, G. E. *Electronics* 1965, 38, 114.
3. Packan, P. A. *Science* 1999, 285, 2079.
4. Wilk, G. D.; Wallace, R. M.; Anthony, J. M. *J Appl Phys* 2001, 89, 5243.
5. Campbell, S. A.; Gilmer, D. C.; Wang, X. C.; Hsieh, M. T.; Kim, H. S.; Gladfelter, W. L.; Yan, J. H. *IEEE Trans Electron Device* 1997, 44, 104.
6. Taylor, C. J.; Gilmer, D. C.; Colombo, D. G.; Wilk, G. D.; Campbell, S. A.; Roberts, J.; Gladfelter, W. L. *J Am Chem Soc* 1999, 121, 5220.
7. Zhang, J.; Yuan, J. S.; Ma, Y.; Oates, A. S. *Solid-State Electron* 2000, 44, 2165.
8. Kadoshima, M.; Hiratani, M.; Shimamoto, Y.; Torii, K.; Miki, H.; Kimura, S.; Nabatame, T. *Thin Solid Films* 2003, 424, 224.
9. Giauque, P. H.; Cherry, H. B.; Nicolet, M. A. *Microelectron Eng* 2001, 55, 183.
10. Sarkar, D. K.; Desbiens, E.; El Khakani, M. A. *Appl Phys Lett* 2002, 80, 294.

11. Smith, R. C.; Hoilien, N.; Dykstra, C.; Campbell, S. A.; Roberts, J. T.; Gladfelter, W. L. *Chem Vap Deposition* 2003, 9, 79.
12. Rignanese, G.-M.; Gonze, X.; Pasquarello, A. *Phys Rev B* 2001, 64, 134301.
13. Rignanese, G.-M.; Gonze, X.; Pasquarello, A. *Phys Rev B* 2001, 63, 104305.
14. Zhao, X.; Vanderbilt, D. *Phys Rev B* 2002, 65, 233106.
15. Zhao, X.; Vanderbilt, D. *Phys Rev B* 2002, 65, 075105.
16. Fiorentini, V.; Gulleri, G. *Phys Rev Lett* 2002, 89, 266101.
17. Rignanese, G.-M.; Detraux, F.; Gonze, X.; Bongiorno, A.; Pasquarello, A. *Phys Rev Lett* 2002, 89, 117601.
18. Rignanese, G.-M.; Gonze, X.; Jun, G.; Cho, K. J.; Pasquarello, A. Submitted for publication.
19. Amos, R. D. In *Ab Initio Methods in Quantum Chemistry*; I, Lawley, K. P., Ed.; Wiley, New York, 1987; Vol. I, p 99.
20. Gonze, X.; Beuken, J.-M.; Caracas, R.; Detraux, F.; Fuchs, M.; Rignanese, G.-M.; Sindic, L.; Verstraete, M.; Zerah, G.; Jollet, F.; Torrent, M.; Roy, A.; Mikami, M.; Ghosez, Ph.; Raty, J.-Y.; Allan, D. C. *Comput Mater Sci* 2002, 25, 478; <http://www.abinit.org>.
21. Perdew, J. P.; Wang, Y. *Phys Rev B* 1992, 45, 13244.
22. Ceperley, D. M.; Alder, B. J. *Phys Rev Lett* 1980, 45, 566.
23. Troullier, N.; Martins, J. L. *Phys Rev B* 1991, 43, 1993.
24. Teter, M. P. *Phys Rev B* 1993, 48, 5031.
25. Monkhorst, H. J.; Pack, J. D. *Phys Rev B* 1976, 13, 5188.
26. Greenwood, N. N.; Earnshaw, A. *Chemistry of Elements*, 2nd ed.; Butterworth-Heinemann: Oxford, UK, 1997; p 957.
27. Abrahams, S. C.; Bernstein, J. L. *J Chem Phys* 1971, 55, 3206.
28. Lee, C.; Ghosez, Ph.; Gonze, X. *Phys Rev B* 1994, 50, 13379.
29. Gonze, X.; Lee, C. *Phys Rev B* 1997, 55, 10355.
30. Ghosez, Ph.; Michenaud, J.-P.; Gonze, X. *Phys Rev B* 1998, 58, 6224.
31. Lee, C.; Gonze, X. *Phys Rev Lett* 1994, 72, 1686.
32. Rousseau, D. L.; Bauman, R. P.; Porto, S. P. S. *J Raman Spectrosc* 1981, 10, 253.
33. Gonze, X.; Charlier, J.-C.; Allan, D. C.; Teter, M. P. *Phys Rev B* 1994, 50, 13035.
34. Giannozzi, P.; de Gironcoli, S.; Pavone, P.; Baroni, S. *Phys Rev B* 1991, 43, 7231.
35. Pecharrromán, C.; Ocaña, M.; Serna, C. J. *J Appl Phys* 1996, 80, 3479.
36. Negita, K. *Acta Metall* 1989, 37, 313.
37. Negita, K.; Takao, H. *J Phys Chem Solids* 1989, 50, 325.
38. Dawson, P.; Hargreave, M. M.; Wilkinson, G. R. *J Phys C: Solid State Phys* 1971, 4, 240.
39. Maradudin, A. A.; Montroll, E. W.; Weiss, G. H.; Ipatova, I. P. In *Solid State Physics: Advances in Research and Applications*; Ehrenreich, H. E., Seitz, F., Turnbull, D., Eds.; Academic: New York, 1971; Suppl. 3, Chap. 4.
40. Filippetti, A.; Spaldin, N. A. *Phys Rev B* 2003, 68, 045111.

Erratum: Titanium Oxides and Silicates as High- κ Dielectrics: A First-Principles Investigation

**G.-M. RIGNANESE,¹ X. ROCQUEFELTE,¹ X. GONZE,¹
ALFREDO PASQUARELLO²**

¹*Unité de Physico-Chimie et de Physique des Matériaux, Université Catholique de Louvain, 1 Place Croix du Sud, B-1348 Louvain-la-Neuve, Belgium, and Research Center on Microscopic and Nanoscopic Materials and Electronic Devices (CERMIN), Université Catholique de Louvain, B-1348 Louvain-la-Neuve, Belgium*

²*Institut de Théorie des Phénomènes Physiques (ITP), Ecole Polytechnique Fédérale de Lausanne (EPFL), CH-1015 Lausanne, Switzerland, and Institut Romand de Recherche Numérique en Physique des Matériaux (IRRMA), CH-1015 Lausanne, Switzerland*

*Published online 28 March 2005 in Wiley InterScience (www.interscience.wiley.com).
DOI 10.1002/qua.20643*

Article in Int J Quantum Chem 2005, 101, 793–801

In the caption of Table V, the conversion factor for the oscillator strengths is wrong: $1 \text{ au} = 253.2638413 \text{ m}^3/\text{s}^2$. This correction does not affect the main results and conclusions. We are sorry for any inconvenience this may have caused.